

Numerical schemes to reconstruct three dimensional time-dependent point sources of acoustic waves [preprint]

Bo Chen^a, Yukun Guo^b, Yao Sun^{a,*}

^aCollege of Science, Civil Aviation University of China, Tianjin, China

^bSchool of Mathematics, Harbin Institute of Technology, Harbin, China

Abstract

This paper is concerned with the numerical simulation of the three dimensional time-dependent inverse source problem of acoustic waves. The modified method of fundamental solutions (MMFS), which expands the solution utilizing the time convolution of the Green's function and the signal function, are proposed to reconstruct both multiple stationary point sources and a moving point source. For the reconstruction of a moving point source, moreover, the MMFS is simplified as a simple sampling method at each time steps. Numerical experiments are provided to show the effectiveness of the proposed methods.

Keywords: time dependent, inverse source problem, wave equation, moving source point, sampling method

1. Introduction

The inverse problems for partial differential equations appear in various fields of science and engineering, and have been extensively studied in the past decades [19, 23, 25]. Among them, the inverse source problem, especially the identification of moving sources, has a wide range of applications such as under water sonar [28, 29], sound simulation and sound source localization [20, 30].

For the reconstruction of stationary sources, the inverse source problem with sources $\delta(t)g(x)$ that are delta-like in time and of limited oscillation in space and sources $q(t)\delta(\partial G)$ that are oscillation in time and delta-like on the boundary of a region in space are considered in [13] and [36], respectively. Uniqueness analysis related to the Helmholtz equation and the phaseless data is shown in [40, 41]. The stability analysis and identification of multiple point sources for the time-harmonic case are considered in [2, 4]. The conditional stability estimate of the wave equation on a line related to the inverse source problem is provided by [11, 12]. The reconstruction of acoustic sources using multiple frequency data of one observation point is analyzed in [3], and a variety of multi-frequency inverse source problems are carefully analyzed in [7, 8, 27, 39]. Analysis of random sources can be seen in [5, 26]. Time-dependent inverse source problems in elastodynamics are analyzed in [6].

*Corresponding Author. College of Science, Civil Aviation University of China, 2898 Jinbei Road, Dongli District, Tianjin 300300, China; syhf2008@gmail.com

For the reconstruction of a moving point source, analysis of the wave equation and direct identifications for the location of the moving point source are studied in [31, 37]. An analysis of the moving point source when the velocity of the source becomes comparable to the speed of wave propagation can be seen in [15]. Matched-filter imaging method and correlation-based imaging for small fast moving debris with constant velocity are analyzed in [14]. A gesture-based input technique with the electromagnetic wave is analyzed in [22]. Unique determination of moving sources in electrodynamics with partial boundary data and initial knowledge of the temporal source function are analyzed in [18].

The method of fundamental solutions (MFS) is a meshless method which expands the solution utilizing the fundamental solutions [1, 33, 10]. The property of the fundamental solution [35], or the Green's function, is the theoretical basis of the MFS. For the three dimensional wave equation, however, the corresponding Green's function involves the Dirac delta distribution, thus the MFS is no longer feasible. Failing for direct applications, the Green's function of the d'Alembert operator $c^{-2}\partial_{tt} - \Delta$ usually appears in a time convolution, such as in the retarded layer potentials [9, 17, 32]. Therefore, instead of the Green's function, a new group of bases given by the time convolution of the Green's function and the signal function are employed in the modified method of fundamental solutions (MMFS) proposed in this paper. For the reconstruction of a moving point source, the MMFS should be computed for each discrete time. Moreover, the MMFS can be simplified to a simple sampling method at each time steps, which is also an important class of methods in the numerical computation of the inverse problems [16, 21, 23, 24, 42].

The time convolution of the Green's function and the signal function is an invaluable tool for the analysis of the time domain scattering problems. Therefore, the MMFS has important significance in the theory of the time domain analysis. Moreover, the proposed methods are feasible to reconstruct both multiple stationary point sources and a moving point source. The numerical implementation of the proposed methods is simple, and extensive experiments are provided to show the effectiveness of the methods. Among them, an experiment to reconstruct a handwritten Chinese character is provided, which is meaningful in practical applications such as the gesture recognition. The outline of this paper is as follows. In Section 2, the inverse source problem with multiple stationary point sources is considered. The uniqueness result with the measurement data on a spherical surface is proved and the MMFS is proposed. In Section 3, the MMFS is applied to the inverse source problem with a moving point source. Moreover, the method is simplified as a simple sampling method at each discrete time. In Section 4, extensive numerical experiments are provided to show the effectiveness of the proposed methods. Finally, the conclusion remarks are given in Section 5.

2. Reconstruction of stationary point sources

Consider the wave equation

$$c^{-2}\partial_{tt}u(x, t) - \Delta u(x, t) = f(x, t), \quad x \in \mathbb{R}^3, t \in \mathbb{R}, \quad (1)$$

where $\partial_{tt}u = \frac{\partial^2 u}{\partial t^2}$, Δ is the Laplacian and $c > 0$ denotes the sound speed of the homogeneous background medium. Denote by $\Omega \subset \mathbb{R}^3$ a bounded convex region with boundary Γ . The source term is

$$f(x, t) := \lambda(t) \sum_{j=1}^M a_j \delta(x - s_j), \quad (2)$$

where $s_j \in \Omega$ are stationary source points, $a_j > 0$ are real constants, M is a positive integer, δ is the Dirac delta distribution and $\lambda(t)$ is a signal function. It is generally assumed that the sources are sparsely distributed and the magnitudes of a_j are of the same order (refer to [42]).

In this paper, the source points s_j are assumed to be mutually distinct. The signal function $\lambda(t)$ is assumed to be causal, which means $\lambda(t) = 0$ for $t < 0$. Thus the source term $f(t) = 0$ for $t < 0$, and the initial condition

$$u(\cdot, 0) = \partial_t u(\cdot, 0) = 0 \quad \text{in } \mathbb{R}^3 \quad (3)$$

is a direct conclusion of the causality.

The inverse source problem (P1) under consideration is: Determine the location and intensity of the stationary point sources from the measurement data

$$u(x, t), \quad x \in \Gamma, t \in \mathbb{R}. \quad (4)$$

Notice that the boundary Γ is the measurement surface where the sensors are located. Assuming that Γ is chosen as the boundary of some convex region, we have the following uniqueness result for the inverse source problem (P1).

Theorem 2.1. *Assume that*

$$f_i(x, t) = \lambda(t) \sum_{j=1}^{M_i} a_j^{(i)} \delta(x - s_j^{(i)}), \quad i = 1, 2$$

are two solutions of the inverse source problem (P1), where M_i are positive integers, $s_j^{(i)} \in \Omega$ are stationary source points, $a_j^{(i)} > 0$ are real constants, and $\lambda(t) \in C(\mathbb{R})$ is a non-trivial causal signal function. Then we have

$$f_1(x, t) = f_2(x, t), \quad \forall (x, t) \in \Omega \times \mathbb{R},$$

that is, $M_1 = M_2 = M$ and $a_j^{(1)} = a_{\pi(j)}^{(2)}$, $s_j^{(1)} = s_{\pi(j)}^{(2)}$, $j = 1, 2, \dots, M$ for some permutation $\pi(j)$ of $1, 2, \dots, M$.

Proof. Assume that u_1 and u_2 are, respectively, the causal wave fields satisfying the wave equation (1) corresponding to the source terms f_1 and f_2 . Denote $w := u_1 - u_2$. Then

$$c^{-2} \partial_{tt} w - \Delta w = f_1 - f_2 \quad \text{in } \mathbb{R}^3 \times \mathbb{R}, \quad (5)$$

$$w = 0 \quad \text{on } \Gamma \times \mathbb{R}. \quad (6)$$

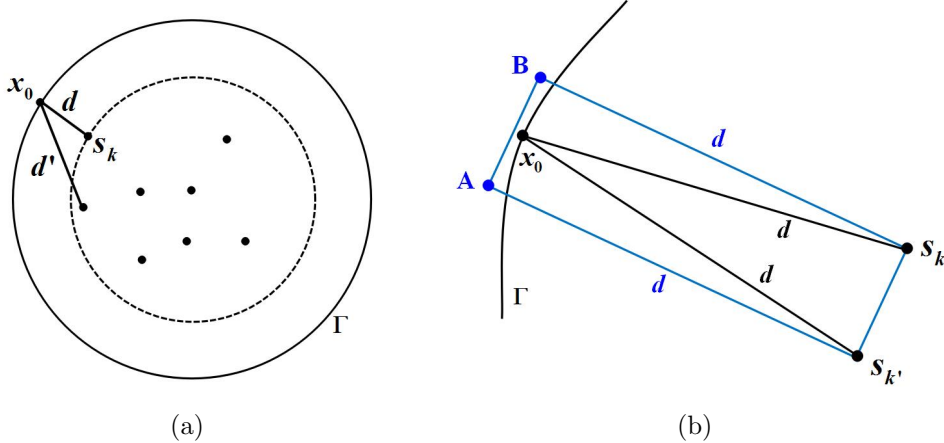


Figure 1: Sketch of the measurement surface and the source points.

It is well known that

$$w_0(x, t) := \sum_{j=1}^{M_1} a_j^{(1)} G(x, t; s_j^{(1)}) * \lambda(t) - \sum_{j=1}^{M_2} a_j^{(2)} G(x, t; s_j^{(2)}) * \lambda(t)$$

is the unique causal solution of the equation (5), where

$$G(x, t; y) = \frac{\delta(t - c^{-1}|x - y|)}{4\pi|x - y|}$$

signifies the Green's function of the d'Alembert operator $c^{-2}\partial_{tt} - \Delta$ and

$$G(x, t; y) * \lambda(t) = \frac{\lambda(t - c^{-1}|x - y|)}{4\pi|x - y|}$$

denotes the time convolution of G and λ .

Notice that w_0 can be rewritten as

$$w_0(x, t) = \sum_{l=1}^{M_0} b_l G(x, t; s_l) * \lambda(t), \quad x \in \Omega, t \in \mathbb{R},$$

where the source points $s_l \in S_d := \bigcup_{i=1,2} \left\{ s_j^{(i)} \right\}_{j=1}^{M_i}$, $M_0 \leq M_1 + M_2$ is the cardinal number of S_d and the coefficients $b_l = \sum_{(i,j) \in E(i,j;l)} (-1)^{i-1} a_j^{(i)}$ with $E(i, j; l) := \{(i, j) : s_j^{(i)} = s_l\}$.

Note that b_l can be zero. As is shown in Figure 1(a), assume that the distance between the set S_d and the boundary Γ is

$$d := \min_{x \in \Gamma, s \in S_d} |x - s| = |x_0 - s_k|,$$

in which $1 \leq k \leq M_0$ and $x_0 \in \Gamma$.

Moreover, we assert that

$$d' := \min_{s \in S_d \setminus \{s_k\}} |x_0 - s| > d.$$

Firstly, it is obvious that $d' \geq d$. Then, by reduction to absurdity, assume that $d' = |x_0 - s_{k'}| = d$ for some $s_{k'} \in S_d \setminus \{s_k\}$. As is shown in Figure 1(b), create a rectangle $s_k s_{k'} AB$ with $s_{k'} A = d$. Then $s_k B = s_{k'} A = d = \min_{x \in \Gamma, s \in S_d} |x - s|$ implies that $A, B \in \bar{\Omega}$.

Thus the rectangle $s_k s_{k'} AB \subset \bar{\Omega}$ for the closed convex region $\bar{\Omega}$. Spin $s_k s_{k'} AB$ around the segment AB to get a cylinder V . Then there exists a $\delta > 0$ such that $B_\delta(x_0) := \{x : |x - x_0| < \delta\} \subset V \subset \bar{\Omega}$, which is a contradiction to $x_0 \in \Gamma$.

Take into consideration the causality, assume that $\lambda(t) = 0$ for $t \leq t_1$ and $\lambda(t) \neq 0$ for $t_1 < t < t_1 + \tau$ with some $t_1 > 0$, $\tau > 0$. Moreover, the wave field satisfies

$$w_0(x_0, t) = b_k \frac{\lambda(t - c^{-1}|x_0 - s_k|)}{4\pi|x_0 - s_k|}, \quad t_1 + c^{-1}d < t < t_1 + c^{-1}d'.$$

Apparently $\lambda(t - c^{-1}|x_0 - s_k|)$ is nontrivial for $t \in (t_1 + c^{-1}d, t_1 + c^{-1}d')$. Then the measurement data (6) implies $b_k = 0$. Thus the solution of (5)-(6) can be rewritten as

$$w_0(x, t) = \sum_{l=1}^{M_0-1} b_l G(x, t; s_l) * \lambda(t) \quad x \in \Omega, t \in \mathbb{R}.$$

Following this procedure, we can finally get $w_0 = 0$, which implies $f_1(x, t) = f_2(x, t)$. Moreover, the fact that $s_j^{(i)}$ are distinct and the linear independence of the Dirac delta distributions imply $M_1 = M_2 = M$ and $a_j^{(1)} = a_{\pi(j)}^{(2)}$, $s_j^{(1)} = s_{\pi(j)}^{(2)}$, $j = 1, 2, \dots, M$ for some permutation $\pi(j)$ of $1, 2, \dots, M$. \square

The classic MFS expands the solution utilizing the Green's function (refer to [33, 34, 38]). However, since the Green's function of the d'Alembert operator involves the Dirac delta distribution, the MFS is not feasible to solve the three dimensional wave equation. Hence, consider the expansion

$$u(x, t) = \sum_{l=1}^{N_z} c(z_l) G(x, t; z_l) * \lambda(t), \quad (7)$$

where N_z is a positive integer, $z_l \in \Omega$ are the chosen sampling points in the sampling region $D \subset \Omega$ and $c(z_l)$ are unknown coefficients to be computed.

The expansion (7) leads to the first modified method of fundamental solutions (MMFS1). We introduce the following proposition related to the modified method under a strong hypothesis.

Proposition 2.1. *Assuming that $c(z_l)$, $l = 1, 2, \dots, N_z$ solve*

$$\sum_{l=1}^{N_z} c(z_l) G(x, t; z_l) * \lambda(t) = u(x, t), \quad x \in \Gamma, t \in \mathbb{R}, \quad (8)$$

where Γ is the boundary of a convex region Ω , N_z is a positive integer, $z_l \in \Omega$ are the sampling points, $\lambda(t) \in C(\mathbb{R})$ is a non-trivial causal signal function, and $u(x, t)$ is a causal wave field satisfies

$$c^{-2}\partial_{tt}u(x, t) - \Delta u(x, t) = \lambda(t) \sum_{j=1}^M a_j \delta(x - s_j), \quad x \in \mathbb{R}^3, t \in \mathbb{R}, \quad (9)$$

where M is a positive integer, $s_j \in \Omega$ are stationary source points and $a_j > 0$ are real constants. Denote $S_d := \{s_j\}_{j=1}^M$ and $Z_d := \{z_l\}_{l=1}^{N_z}$. Then $S_d \subset Z_d$. Moreover, $c(z_l) = a_j$ for $z_l = s_j \in S_d$ and $c(z_l) = 0$ for $z_l \in Z_d \setminus S_d$.

Proof. Notice that

$$u(x, t) = \sum_{j=1}^M a_j G(x, t; s_j) * \lambda(t) \quad (10)$$

is the unique causal solution of the wave equation (9). The wave field

$$u'(x, t) = \sum_{l=1}^{N_z} c(z_l) G(x, t; z_l) * \lambda(t), \quad x \in \mathbb{R}^3, t \in \mathbb{R}.$$

is a causal solution of

$$c^{-2}\partial_{tt}u(x, t) - \Delta u(x, t) = \lambda(t) \sum_{l=1}^{N_z} c(z_l) \delta(x - z_l), \quad x \in \mathbb{R}^3, t \in \mathbb{R}.$$

Moreover, the assumption (8) implies

$$u'(x, t) = u(x, t), \quad x \in \Gamma, t \in \mathbb{R},$$

Then the conclusion follows from Theorem 2.1. \square

The MMFS1 to solve the inverse source problem (P1) is shown in Algorithm I. The numerical application of Algorithm I can be seen in Section 4.

3. Reconstruction of a moving point source

In this section, the inverse source problem with a moving point source is considered. The wave equation is

$$c^{-2}\partial_{tt}u(x, t) - \Delta u(x, t) = \lambda(t) \delta(x - s(t)), \quad x \in \mathbb{R}^3, t \in \mathbb{R}, \quad (11)$$

where $s : [0, T] \rightarrow \mathbb{R}^3$ signifies the smooth trajectory of the moving point source. Assume that for any fixed $t \in [0, T]$, the location $s(t) \in \Omega$ and $s(t) \notin \Gamma$. Denote by

$$v(t) = \frac{ds(t)}{dt}$$

Algorithm I. MMFS to reconstruct stationary point sources

- Step 1** Choose a measurement surface Γ , a signal function $\lambda(t)$, an integer M and the locations s_j ($j = 1, \dots, M$) of the point sources. Collect the wave data $u(x_i, t_k)$ for each sensing points $x_i \in \Gamma$ ($i = 1, \dots, N_x$) and discrete time steps $t_k \in [0, T]$ ($k = 1, \dots, N_T$), where T is a chosen terminal time.
- Step 2** Choose a sampling region $D \subset \Omega$ such that $s_j \in D$ and $D \cap \Gamma = \emptyset$. Select a grid of sampling points z_l ($l = 1, \dots, N_z$) in D . Compute $c(z_l)$ from
- $$\sum_{l=1}^{N_z} c(z_l)(G * \lambda)(x_i, t_k; z_l) = u(x_i, t_k), \quad i = 1, \dots, N_x, k = 1, \dots, N_T$$
- using the conjugate gradient method.
- Step 3** Mesh $c(z_l)$ on the sampling grid. The locations of the point sources are given by the locations of z_l for which $c(z_l)$ are local maximum values.
-

the instantaneous velocity of the point source. Again, the initial condition follows from the causality of $\lambda(t)$.

The inverse source problem (P2) with a moving point source is: Determine the trajectory $s(t)$ of the moving point source from the wave equation (11) and the measurement data (4).

The MMFS1 is feasible to reconstruct stationary point sources. However, for a moving point source, the location of the point source changes with time. Thus the coefficients $c(z_l)$ in the MMFS1 should also depend on the time variable t . Therefore, consider a new expansion

$$u(x, t) = \sum_{l=1}^{N_z} c(t; z_l)G(x, t; z_l) * \lambda(t), \quad z_l \in \Omega, \quad (12)$$

where $z_l \in \Omega$ are the sampling points and $c(t; z_l)$ are unknown functions of t depending on z_l . The second modified method of fundamental solutions (MMFS2) for the reconstruction of the moving point source is based on the expansion (12). The algorithm of MMFS2 is similar to Algorithm I except that a new expansion (12) is employed and $c(t_k; z_l)$, $l = 1, \dots, N_z$ are computed respectively for each time steps t_k .

Notice that there is only a single point source in this case. If $|v| = 0$, referring to the analysis of Proposition 2.1, $c(t_k; z_l) \neq 0$ only when $z_l = s(t_k)$ for any $t_k \in [0, T]$. Moreover, $c(t_k; s(t_k)) = 1$. Basing on this, we expect that $G(x, t; s(t_k)) * \lambda(t)$ is the approximation of $u(x, t_k)$ when $|v|$ is small. Then the MMFS2 is in fact equivalent to a simple sampling method.

Define the indicator function

$$I(z, t) = \frac{1}{\|u_0(x, t; s(t)) - G(x, t; z) * \lambda(t)\|}, \quad x \in \Gamma, t \in [0, T], \quad (13)$$

where $\|\cdot\|$ is the $L^2(\Gamma)$ norm with respect to x . We have the following theorem concerning the indicator function (13).

Theorem 3.1. Assume that $d_\Omega \ll c$, $|v| \ll c$ and $\lambda, s \in C^1[0, T]$. Let $u_0(x, t)$ be the causal solution of the wave equation (11). For any fixed $t \in [0, T]$, the indicator function (13) satisfies:

$$I(z, t) \rightarrow +\infty \quad \text{when } z \rightarrow s(t).$$

Proof. Note that when $|v(t)| < c$, $\forall t \in (0, T)$, the explicit solution to equation (11) is given by (refer to [31])

$$u_0(x, t) = \frac{\lambda(\tau)}{4\pi|x - s(\tau)| \left(1 - \frac{v(\tau) \cdot (x - s(\tau))}{c|x - s(\tau)|}\right)}, \quad (14)$$

where the retarded time τ satisfies $t - \tau = c^{-1}|x - s(\tau)|$.

Under the assumptions $d_\Omega \ll c$, $|v| \ll c$ and $\lambda, s \in C^1[0, T]$, we assert that

$$G(x, t; s(t)) * \lambda(t) = \frac{\lambda(t - c^{-1}|x - s(t)|)}{4\pi|x - s(t)|}$$

is an approximation of the solution (14). The proof of a similar conclusion can be seen in [37]. Though we use an arbitrary causal signal function $\lambda(t)$ instead of the time-harmonic signal $\lambda(t) = \sin(\omega_0 t)$ in [37] for some $\omega_0 > 0$, and the function $\lambda(t - c^{-1}|x - s(t)|)$ is occupied in $G(x, t; s(t)) * \lambda(t)$ instead of $\lambda(t)$, a similar discussion as that in [37] implies

$$u_0(x, t) = G(x, t; s(t)) * \lambda(t) + O(\varepsilon(t)), \quad x \in \Gamma, t \in [0, T],$$

where $0 < \varepsilon(t) \ll 1$.

Then the smoothness of the function $G(x, t; z) * \lambda(t)$ with respect to z implies the conclusion. \square

Then we get Algorithm II, a simplified scheme to solve the inverse source problem (P2). The numerical implement of Algorithm II is shown in Section 4.

Algorithm II. The simplified scheme to reconstruct a moving point source

Step 1 Choose a measurement surface Γ , a signal function $\lambda(t)$ and the trajectory $s(t), t \in [0, T]$ of the moving point source. Collect the wave data $u(x_i, t_k)$ on each sensing points $x_i \in \Gamma$ ($i = 1, \dots, N_x$) and discrete time steps t_k ($k = 1, \dots, N_T$).

Step 2 Choose a sampling region D such that $s_j \in D$ and $D \cap \Gamma = \emptyset$. Select a grid of sampling points z_l ($l = 1, \dots, N_z$) in D . For each time step t_k , compute

$$I(z_l, t_k) = \left(\sum_{i=1}^{N_x} ((G * \lambda)(x_i, t_k; z_l) - u(x_i, t_k))^2 \right)^{-1/2}.$$

Step 3 For each time step t_k , the location $s(t_k)$ of the point source is approximated by the location of z_l for which $I(z_l, t_k)$ is the global maximum value.

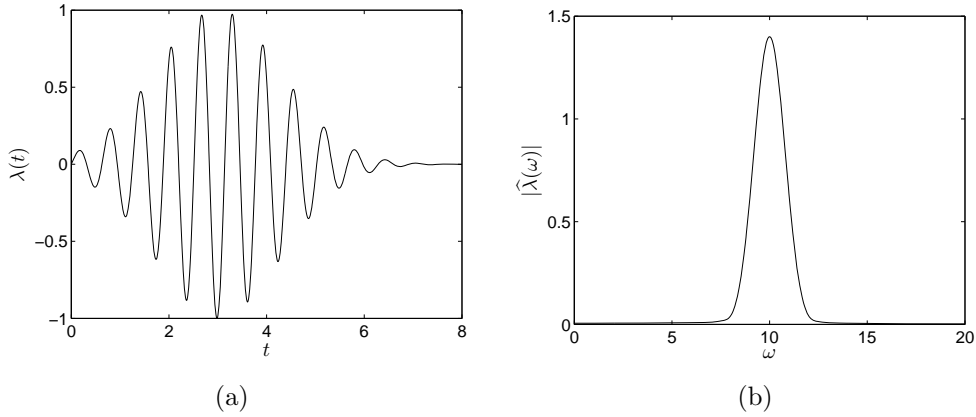


Figure 2: (a) The pulse function $\lambda(t) = \sin(10t)e^{-0.3(t-3)^2}$. (b) The Fourier spectrum $|\hat{\lambda}(\omega)|$.

4. Numerical examples

In this section, we consider the numerical implementation of the proposed methods. The radiated field is computed for $t \in [0, T]$, where T is the terminal time. The time discretization is

$$t_n = n \frac{T}{N_T}, \quad n = 0, 1, \dots, N_T.$$

Random noises are added to the data with

$$u_\delta = (1 + \delta r)u,$$

where $\delta > 0$ is the noise level and r are uniformly distributed random numbers in $[-1, 1]$.

In all the experiments, the signal function $\lambda(t)$ is chosen as

$$\lambda(t) = \sin(10t)e^{-0.3(t-3)^2}.$$

The signal function $\lambda(t)$ and its Fourier spectrum can be seen in Figure 2.

4.1. Reconstruction of multiple static point sources

For the reconstruction of multiple static point sources, the sound speed is fixed to be $c = 1$. Algorithm I is employed to reconstruct the sources. The synthetic data is given by the analytic solution (10). The terminal time is chosen as $T = 15$ in this subsection.

Example 1: Assume that a priori knowledge is provided that the point sources are in a plane S . Thus, instead of the radiated field on the measurement surface Γ , only the radiated field on the curve $\Gamma' := S \cap \Gamma$ is sufficient for the reconstruction. The source points are chosen as $(-3/2, 3/2, 0)$, $(-3/2, -1/2, 0)$, $(-1, -1, 0)$, $(-1, -6/5, 0)$, $(-2/3, 3/5, 0)$, $(0, 1, 0)$, $(0, -2/3, 0)$, $(1/3, 1/3, 0)$, $(1, 1/2, 0)$, $(1, 0, 0)$, $(3/2, 3/2, 0)$ and $(3/2, -1, 0)$ with relative intensities 3, 2, 3, 2, 1, 2, 4, 3, 4, 2, 2 and 3, respectively. The sampling points are chosen as 61×61 uniform discrete points on $\{(x_1, x_2, 0) | (x_1, x_2) \in$

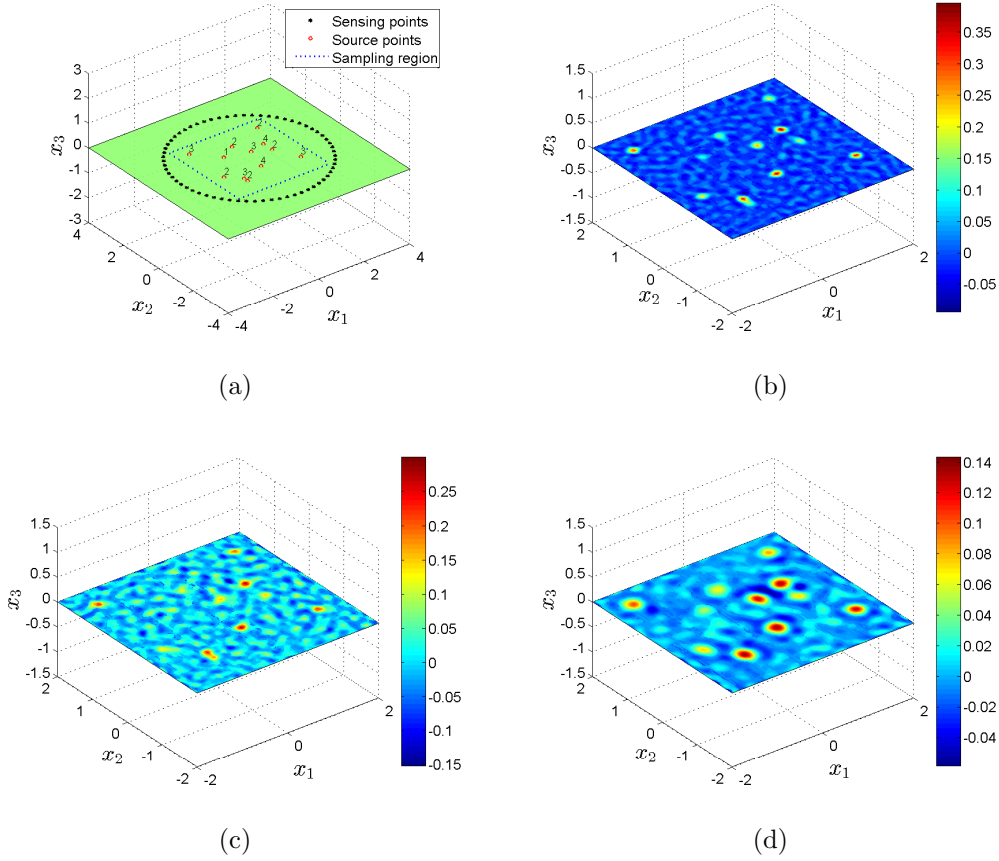


Figure 3: Reconstruction of 12 stationary point sources with different intensities. (a) Sketch of the example. (b) Reconstruction with $\delta = 1\%$, $N_T = 64$. (c) Reconstruction with $\delta = 5\%$, $N_T = 64$. (d) Reconstruction with $\delta = 5\%$, $N_T = 32$.

$[-2, 2] \times [-2, 2]$. The sensing points are $N_x = 64$ equidistant discrete points on the measurement curve $\Gamma'_1 := \{3(\cos \theta, \sin \theta, 0), \theta \in [0, 2\pi)\}$. The reconstruction of the point sources is shown in Figure 3 with different noise levels.

As is shown in Figure 3(b), the proposed method is feasible to reconstruct point sources with different intensities. The reconstruction of the point source with relatively small intensity is also relatively blurry. When the noise level is chosen as $\delta = 5\%$, only the point sources with relatively large intensities can be recognized from the reconstruction. Figure 3(c) and Figure 3(d) show the reconstructions when $\delta = 5\%$ respectively with $N_T = 64$ and with $N_T = 32$. As we can see from the figure, the reconstruction is more clear when $N_T = 32$ in some sense.

Remark 4.1. *The reconstruction is more sensitive to noise when the intensities of the point sources are with larger contrasts. As is shown in Example 1, the influence of the noise is expanded for the reconstruction of the point sources with small relative intensity.*

Moreover, the reconstruction with sensors on semicircles can be seen in Figure 4. As is shown in the figure, the reconstruction of the point sources in the semicircle region

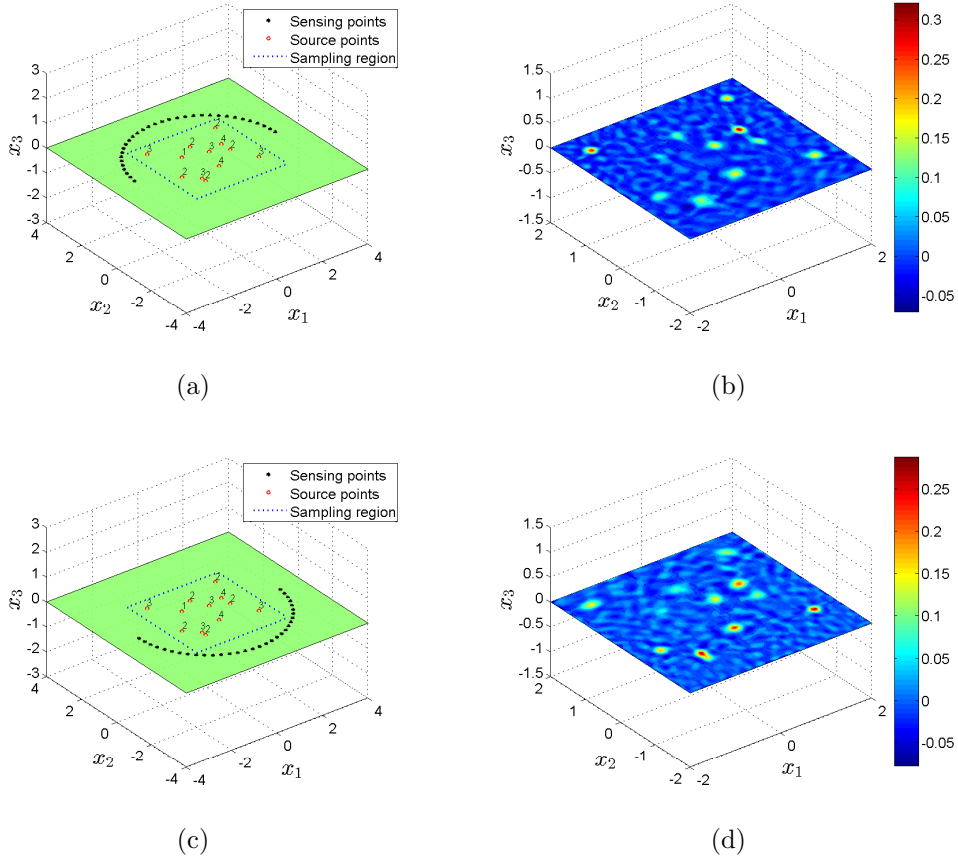


Figure 4: Reconstruction of stationary point sources with part of the sensors, $N_T = 64$. (a) Sketch of Case 1. (b) Reconstruction of Case 1, $\delta = 1\%$. (c) Sketch of Case 2. (d) Reconstruction of Case 2, $\delta = 1\%$.

with sensors on the boundary is better than the reconstruction of the point sources outside the semicircle region.

Example 2: In this example, the reconstruction of the stationary point sources $(0, -1, 1)$, $(0, 1, -1)$, $(1, -1, 0)$ and $(1, 0, -1)$ with the same intensity is provided. The sensing points are discrete points $(5 \sin \varphi_i \cos \theta_j, 5 \sin \varphi_i \sin \theta_j, 5 \cos \varphi_i)$ with $\varphi_i = \frac{2i-1}{16}\pi$, $i = 1, 2, \dots, 8$ and $\theta_j = \frac{j}{4}\pi$, $j = 0, 1, \dots, 7$. The sampling points are $21 \times 21 \times 21$ uniform discrete points in $[-2, 2] \times [-2, 2] \times [-2, 2]$. The location of the sensors and the reconstruction are shown in Figure 5.

Remark 4.2. *To facilitate the 3D visualization, we added some 2D projections in the figure.*

4.2. Reconstruction of a moving point source

Subsection 4.2 is concerned with the reconstruction of a moving source. The sound speed is fixed to be $c = 340$ in this subsection. The terminal time is chosen as $T = 2\pi$.

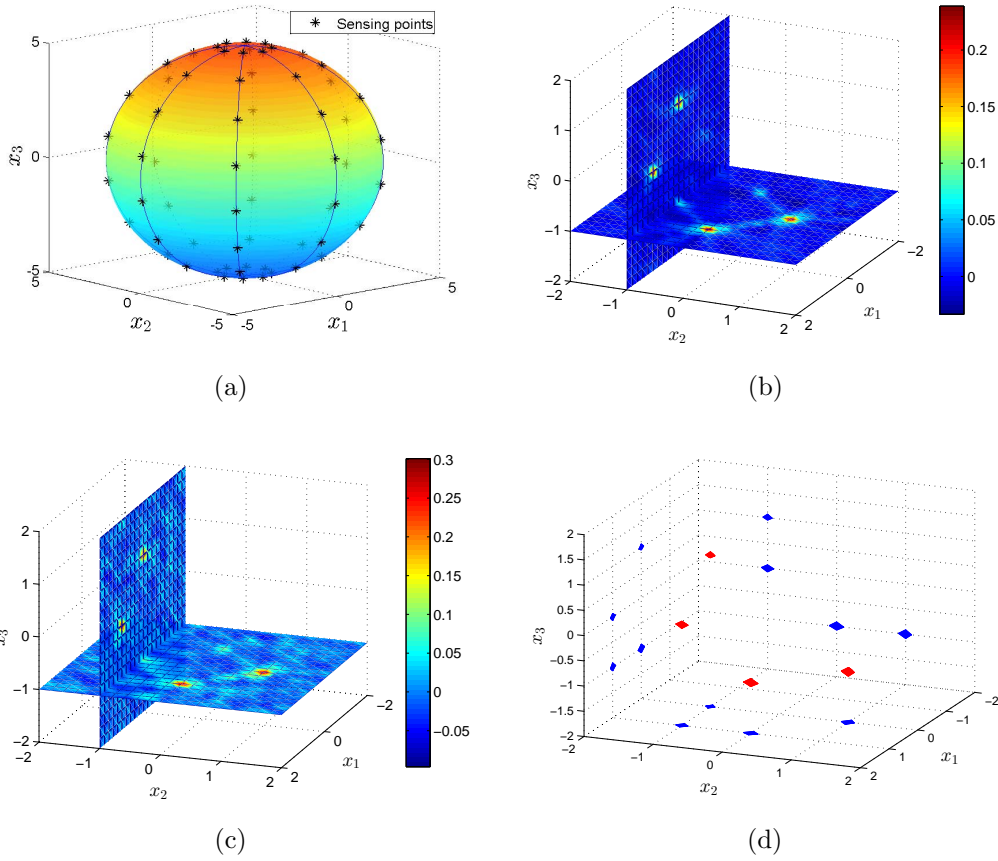


Figure 5: Reconstruction of 4 stationary point sources with the same intensity. (a) Location of the sensors. (b) Reconstruction of the point sources, $\delta = 1\%$. (c) Reconstruction of the point sources, $\delta = 5\%$. (d) The isosurface of the indicator $I(y_j)$ of the value $0.7 \max\{I(y_j)\}$, $\delta = 5\%$.

Numerical scheme based on Algorithm II is employed to reconstruct a moving point source. The measurement data is given by the analytic solution (14).

Example 3: In this example, the trajectory of the moving point source is known to be in a plane S and only the radiated field on $\Gamma' := S \cap \Gamma$ is needed for the reconstruction. The trajectory of the moving source is chosen as $s(t) = (2 + 0.3 \cos 3t)(\cos t, \sin t, 0)$, $t \in [0, T]$. The reconstruction $s'(t_k)$ of the locations $s(t_k)$, $k = 1, 2, \dots, N_T$ are considered. We choose $N_T = 64$ in this experiment.

The sampling points are chosen as 51×51 uniform discrete points in the sampling region $\{(x_1, x_2, 0) | (x_1, x_2) \in [-3, 3] \times [-3, 3]\}$. The sensing points are $N_x = 64$ equidistant discrete points on the measurement curve $\Gamma'_2 := \{5(\cos \theta, \sin \theta, 0), \theta \in [0, 2\pi)\}$. The reconstruction is shown in Figure 6.

As is shown in Figure 6(b), the locations $s'(t_k)$ is close to the trajectory $s(t)$ except for several discrete points. The error given by the Euclidean distance $|s(t) - s'(t)|$ at each discrete time steps t_k can be seen in Figure 6(c). We find that the error becomes large when the signal intensity $\lambda(t_k) = 0$. Therefore, the following modification is provided after the reconstruction:

- (1) If $|\lambda(t_1)| < 10^{-4}$, redefine $s'(t_1) = 2s'(t_2) - s'(t_3)$.
- (2) If $|\lambda(t_{N_T})| < 10^{-4}$, redefine $s'(t_{N_T}) = 2s'(t_{N_T-1}) - s'(t_{N_T-2})$.
- (3) If $|\lambda(t_k)| < 10^{-4}$ for any $k = 2, \dots, N_T - 1$, redefine $s'(t_k) = \frac{1}{2}(s'(t_{k-1}) + s'(t_{k+1}))$.

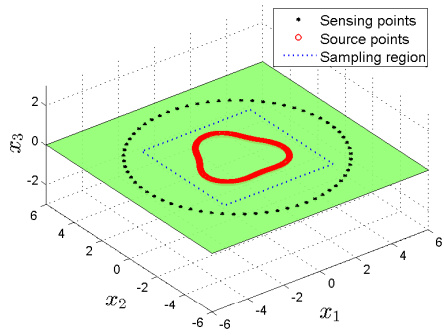
Remark 4.3. *When $\lambda(t_k) = 0$, the approximate solution $(G * \lambda)(x, t_k; z) = 0$, $\forall z \in D$. Thus the reconstruction $s'(t_k)$ is actually meaningless when $\lambda(t_k) = 0$ and the modification is necessary.*

The modified reconstruction and the corresponding error can be seen in Figure 6(d) and Figure 6(e), respectively. As we can see from Figure 6(e), the error $|s(t_k) - s'(t_k)| < 0.2$ after the modification. Thus the modification is applied to all the experiments in the following. Fourier expansion of order 3 is employed to get a smooth reconstruction of the trajectory.

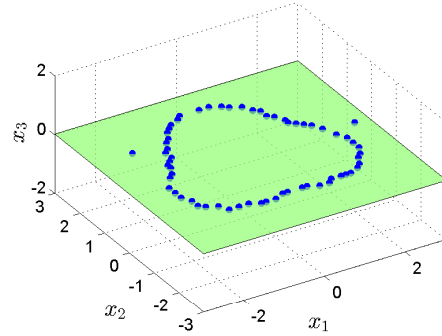
Remark 4.4. *An important component of the error is caused by the discretization precision of the sampling region. Thus there still exists the error $|s(t_n) - s'(t_n)| < 0.2$, which coincides with the 51×51 uniform discretization of the sampling region $[-3, 3] \times [-3, 3]$. The error can be reduced by selecting more sampling points or narrow down the sampling region.*

Example 4: In this example, we consider the reconstruction of arbitrary trajectory of a moving source in \mathbb{R}^3 . The sensors are chosen the same as that in Example 2. The sampling points are chosen as $51 \times 51 \times 51$ uniform discrete points in $[-3, 3] \times [-3, 3] \times [-3, 3]$. We also choose $N_T = 64$ in this experiment.

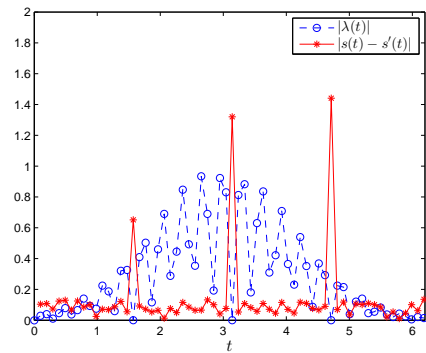
The trajectories of the moving source are chosen as $s(t) = 2(\sin t, \frac{t}{\pi} - 1, 0)$ and $s(t) = 2(\sin(2t), \cos(2t), \frac{t}{\pi} - 1)$, respectively in two cases. The reconstruction can be



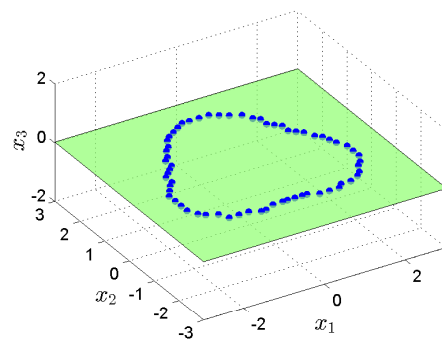
(a)



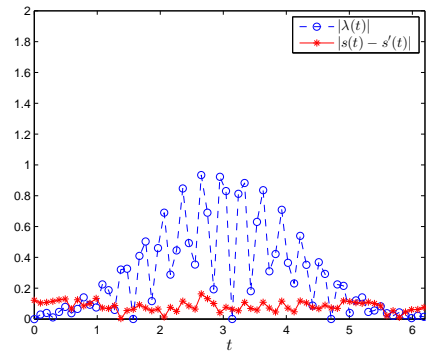
(b)



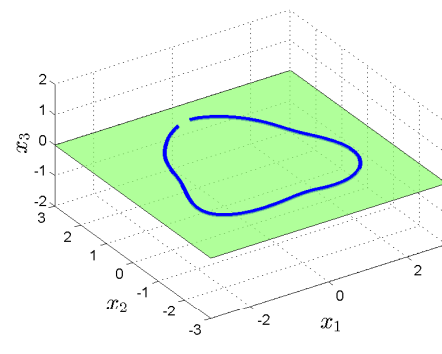
(c)



(d)



(e)



(f)

Figure 6: Reconstruction of a moving point source in a plane. (a) Sketch of the example. (b) The reconstruction points, $\delta = 5\%$. (c) The error of the reconstruction. (d) The modified reconstruction points, $\delta = 5\%$. (e) The error of the modified reconstruction. (f) The smooth reconstruction by the Fourier expansion of order 3.

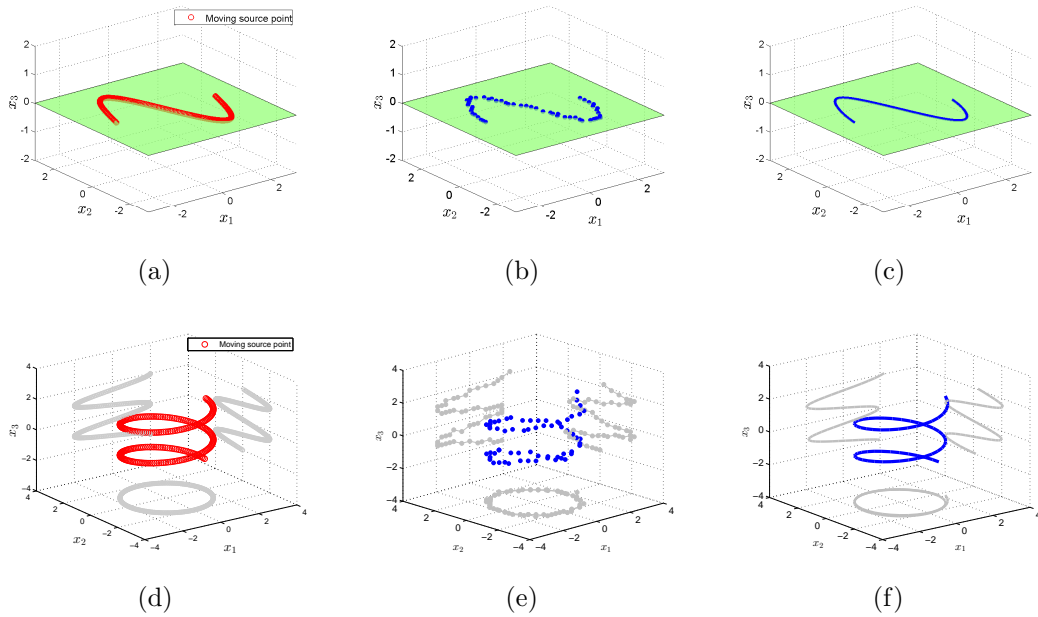


Figure 7: Reconstruction of arbitrary trajectory of the moving source in \mathbb{R}^3 . (a) Trajectory of Case 1. (b) The reconstruction points of Case 1, $\delta = 5\%$. (c) The smooth reconstruction of Case 1 by the Fourier expansion of order 3. (d) Trajectory of Case 2. (e) The reconstruction points of Case 2, $\delta = 5\%$. (f) The smooth reconstruction of Case 2 by the Fourier expansion of order 3.

seen in Figure 7. As is shown in the figure, the algorithm is feasible to reconstruct different trajectories with noise level $\delta = 5\%$.

Remark 4.5. *When there is no priori knowledge that the trajectory of the moving point source is in a plane, the sampling has to be done in a three dimensional region and the computational cost is higher. Even though, the reconstruction is as good as that in Example 3 when the step sizes are the same.*

Example 5: As an addition of Example 4, the reconstruction of a handwritten Chinese character “ai” is considered. We choose $N_T = 128$ in this experiment. The reconstruction can be seen in Figure 8.

The smooth reconstruction in this example is also provided by the Fourier expansion. However, the Chinese character “ai” has 5 strokes and can not be reconstruct by a single smooth curve. Thus the smooth reconstruction basing on the Fourier expansion of each strokes is needed. Since the point source moves faster in the gap between two strokes, we use the following strategy to provide the smooth reconstruction:

- (1) If $\max(|s'(t_{k-1}) - s'(t_k)|, |s'(t_{k+1}) - s'(t_k)|) > 0.3$ for any $k = 2, \dots, N_T - 1$, classify $s'(t_k)$ as the end point of a stroke or the point between two strokes.
- (2) Separate the strokes of the character, and provide the smooth reconstruction of each stroke using the Fourier expansion.

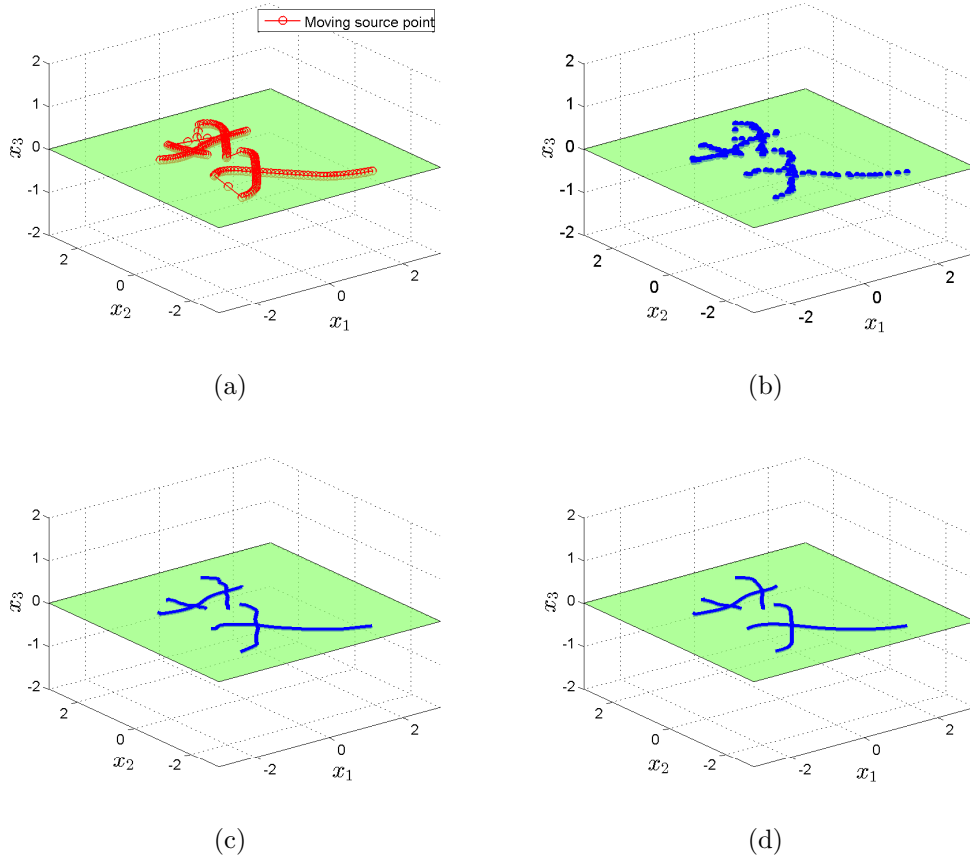


Figure 8: Reconstruction of a handwritten Chinese character “ai”. (a) Trajectory of the point source. (b) The reconstruction points, $\delta = 5\%$. (c) The smooth reconstruction by the Fourier expansion of order 5. (d) The smooth reconstruction by the Fourier expansion of order 3.

As is shown in the figure, the algorithm is feasible to reconstruct the character with noise level $\delta = 5\%$. The smooth reconstructions by the Fourier expansion with order 5 and order 3 are shown in Figure 8(c) and Figure 8(d), respectively.

Remark 4.6. *The separation of strokes relies on the fact that the speed of the point source between two strokes is significantly larger than the speed in a stroke, which is consistent with the reality. The separation of strokes is important since a direct smooth reconstruction by the Fourier expansion shows the Chinese character in one stroke, which causes difficulties for identifying the character.*

Remark 4.7. *The smooth reconstruction by the Fourier expansion of order 5 indeed shows more details of the reconstruction points than that of order 3. However, some of the details are caused by the noises. Therefore, as is shown in Figure 8(c-d), the smooth reconstruction by the Fourier expansion of order 3 is better in this example.*

Example 6: In this example, the reconstruction of arbitrary trajectory using 4 sensors is considered. The sensing points are chosen as $(3, 3, -3)$, $(3, -3, -3)$, $(-3, 3, -3)$ and

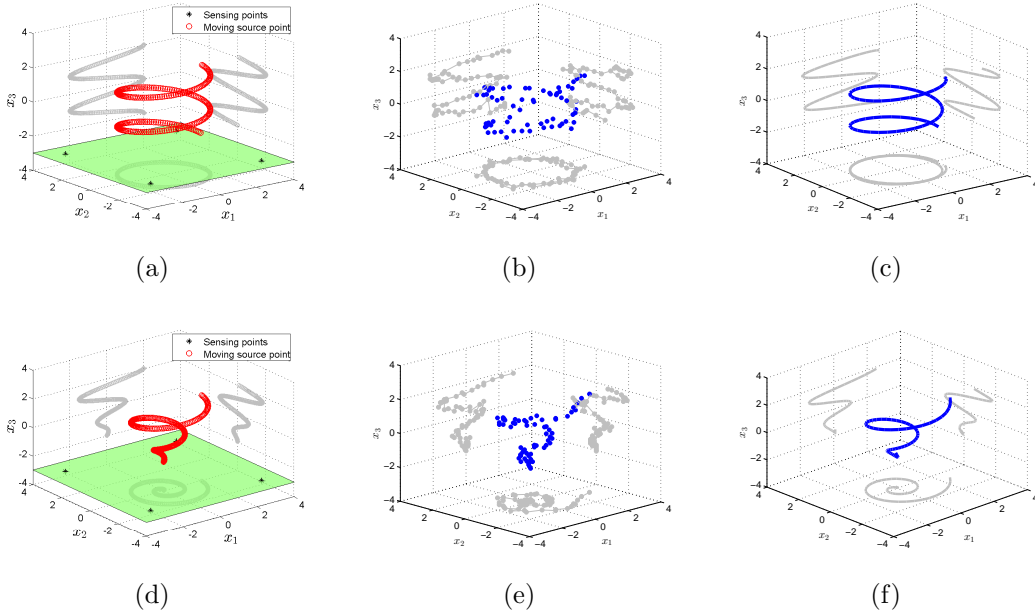


Figure 9: Reconstruction of a moving source with 4 sensors. (a) Sketch of Case 1. (b) The reconstruction points of Case 1. (c) The smooth reconstruction of Case 1 by the Fourier expansion of order 3. (d) Sketch of Case 2. (e) The reconstruction points of Case 2. (f) The smooth reconstruction of Case 2 by the Fourier expansion of order 3.

$(-3, -3, -3)$. The sampling points and the time discretization are chosen the same as that in Example 4.

The trajectories of the moving source are chosen as $s(t) = 2(\sin(2t), \cos(2t), t/\pi - 1)$ and $s(t) = 2(\frac{t}{\pi} \sin(2t), \frac{t}{\pi} \cos(2t), t/\pi - 1)$, respectively in two cases. The reconstruction can be seen in Figure 9.

Remark 4.8. *The error of the reconstruction with only 4 sensors is bigger than that of the previous experiments. However, the smooth reconstruction ignores most of the error and the algorithm still works well with noise level $\delta = 5\%$.*

5. Conclusion

We have considered the numerical simulation of the time dependent inverse source problems of acoustic waves. The modified methods of fundamental solutions (MMFS) have been established to reconstruct both multiple stationary sources and a moving point source. Moreover, the MMFS to reconstruct a moving point source have been modified to a simple sampling method. Plentiful numerical examples have been provided to show the effectiveness of the proposed methods.

Acknowledgements

The work of Bo Chen was supported by the NSFC (No. 11671170) and the Fundamental Research Funds for the Central Universities (Special Project for Civil Aviation

University of China, No. 3122018L009). The work of Yukun Guo was supported by the NSFC (No. 11601107, 41474102 and 11671111). The work of Yao Sun was supported by the NSFC (No. 11501566).

References

References

- [1] M. N. Ahmadabadi, M. Arab, and F. M. M. Ghaini. The method of fundamental solutions for the inverse space-dependent heat source problem. *Engineering Analysis with Boundary Elements*, 33(10):1231–1235, 2009.
- [2] C. Alves, R. Kress, and P. Serranho. Iterative and range test methods for an inverse source problem for acoustic waves. *Inverse Problems*, 25(5):055005, 2009.
- [3] A. Alzaalig, G. Hu, X. Liu, and J. Sun. Fast acoustic source imaging using multi-frequency sparse data. arXiv: 1712.02654.
- [4] A. E. Badia and T. Nara. An inverse source problem for Helmholtz’s equation from the Cauchy data with a single wave number. *Inverse Problems*, 27(10):105001, 2011.
- [5] G. Bao, S. N. Chow, P. Li, and H. Zhou. An inverse random source problem for the Helmholtz equation. *Mathematics of Computation*, 83(285):215–233, 2014.
- [6] G. Bao, G. Hu, Y. Kian, and T. Yin. Inverse source problems in elastodynamics. *Inverse Problems*, 34(4):045009, 2017.
- [7] G. Bao, J. Lin, and F. Triki. A multi-frequency inverse source problem. *Journal of Differential Equations*, 249(12):3443–3465, 2010.
- [8] G. Bao, S. Lu, W. Rundell, and B. Xu. A recursive algorithm for multi-frequency acoustic inverse source problems. *SIAM Journal on Numerical Analysis*, 53(3):1608–1628, 2015.
- [9] B. Chen, F. Ma, and Y. Guo. Time domain scattering and inverse scattering problems in a locally perturbed half-plane. *Applicable Analysis*, 96(8):1303–1325, 2017.
- [10] B. Chen, Y. Sun, and Z. Zhuang. Method of fundamental solutions for a Cauchy problem of the Laplace equation in a half-plane. *Boundary Value Problems*, 2019(34):1–14, 2019.
- [11] J. Cheng, G. Ding, and M. Yamamoto. Uniqueness along a line for an inverse wave source problem. *Communications in Partial Differential Equations*, 27(9-10):2055–2069, 2002.
- [12] J. Cheng, L. Peng, and M. Yamamoto. The conditional stability in line unique continuation for a wave equation and an inverse wave source problem. *Inverse Problems*, 21(6):1993–2007, 2005.
- [13] M. V. De Hoop and J. Tittelfitz. An inverse source problem for a variable speed wave equation with discrete-in-time sources. *Inverse Problems*, 31(7):075007, 2015.
- [14] J. Fournier, J. Garnier, G. Papanicolaou, and C. Tsogka. Matched-filter and correlation-based imaging for fast moving objects using a sparse network of receivers. *Siam Journal on Imaging Sciences*, 10(4):2165–2216, 2017.
- [15] J. Garnier and M. Fink. Super-resolution in time-reversal focusing on a moving source. *Wave Motion*, 53:80–93, 2015.

- [16] Y. Guo, D. Hömberg, G. Hu, J. Li, and H. Liu. A time domain sampling method for inverse acoustic scattering problems. *Journal of Computational Physics*, 314:647–660, 2016.
- [17] Y. Guo, P. Monk, and D. Colton. Toward a time domain approach to the linear sampling method. *Inverse Problems*, 29(9):095016, 2013.
- [18] G. Hu, Y. Kian, P. Li, and Y. Zhao. Inverse moving source problems in electrodynamics. *arXiv:1812.06215*, 2018.
- [19] V. Isakov. *Inverse Problems for Partial Differential Equations*. Springer-Verlag, New York, 1998.
- [20] M. Lassas and L. Oksanen. Inverse problem for wave equation with sources and observations on disjoint sets. *Inverse Problems*, 26(8):085012, 2010.
- [21] J. Li, H. Liu, Z. Shang, and H. Sun. Two single-shot methods for locating multiple electromagnetic scatterers. *SIAM Journal on Applied Mathematics*, 73(4):1721–1746, 2013.
- [22] J. Li, H. Liu, and H. Sun. On a gesture-computing technique using electromagnetic waves. *Inverse Problems and Imaging*, 12:677–696, 2018.
- [23] J. Li, H. Liu, and J. Zou. Multilevel linear sampling method for inverse scattering problems. *Journal of Computational Physics*, 30(3):1228–1250, 2008.
- [24] J. Li, H. Liu, and J. Zou. Strengthened linear sampling method with a reference ball. *SIAM Journal on Scientific Computing*, 31(6):4013–4040, 2009.
- [25] J. Li, H. Liu, and J. Zou. Locating multiple multiscale acoustic scatterers. *SIAM Multiscale Modeling and Simulations*, 12:927–952, 2014.
- [26] P. Li. An inverse random source scattering problem in inhomogeneous media. *Inverse Problems*, 27(3):035004, 2011.
- [27] P. Li and G. Yuan. Increasing stability for the inverse source scattering problem with multi-frequencies. *Inverse Problems and Imaging*, 11(4):745–759, 2016.
- [28] P. H. Lim and J. M. Ozard. On the underwater acoustic field of a moving point source. i. range-independent environment. *Journal of the Acoustical Society of America*, 95(1):131–137, 1994.
- [29] P. H. Lim and J. M. Ozard. On the underwater acoustic field of a moving point source. ii. range-dependent environment. *Journal of the Acoustical Society of America*, 95(1):138–151, 1994.
- [30] M. Matsumoto, M. Tohyama, and H. Yanagawa. A method of interpolating binaural impulse responses for moving sound images. *Acoustical Science and Technology*, 24(5):284–292, 2003.
- [31] E. Nakaguchi, H. Inui, and K. Ohnaka. An algebraic reconstruction of a moving point source for a scalar wave equation. *Inverse Problems*, 28(6):065018, 2012.
- [32] F. J. Sayas. *Retarded Potentials and Time Domain Boundary Integral Equations: a Road-map*. Springer Series in Computational Mathematics, Switzerland, 2016.
- [33] Y. Sun. Modified method of fundamental solutions for the Cauchy problem connected with the Laplace equation. *International Journal of Computer Mathematics*, 91(10):2185–2198, 2014.
- [34] Y. Sun. Indirect boundary integral equation method for the Cauchy problem of the Laplace equation. *Journal of Scientific Computing*, 71(2):469–498, 2017.

- [35] Y. Sun, Y. Guo, and F. Ma. The reciprocity gap functional method for the inverse scattering problem for cavities. *Applicable Analysis*, 95(6):1327–1346, 2016.
- [36] B. A. Ton. An inverse source problem for the wave equation. *Nonlinear Analysis*, 55(3):269–284, 2003.
- [37] X. Wang, Y. Guo, J. Li, and H. Liu. Mathematical design of a novel input/instruction device using a moving emitter. *Inverse Problems*, 33(10):105009, 2017.
- [38] T. Wei and D. Y. Zhou. Convergence analysis for the Cauchy problem of Laplace’s equation by a regularized method of fundamental solutions. *Advances in Computational Mathematics*, 33(4):491–510, 2010.
- [39] D. Zhang and Y. Guo. Fourier method for solving the multi-frequency inverse source problem for the Helmholtz equation. *Inverse Problems*, 31(3):035007, 2015.
- [40] D. Zhang and Y. Guo. Uniqueness results on phaseless inverse scattering with a reference ball. *Inverse Problems*, 34(8):085002, 2018.
- [41] D. Zhang, Y. Guo, J. Li, and H. Liu. Retrieval of acoustic sources from multi-frequency phaseless data. *Inverse Problems*, 34(9):094001, 2018.
- [42] D. Zhang, Y. Guo, J. Li, and H. Liu. Locating multiple multipolar acoustic sources using the direct sampling method. *Communications in Computational Physics*, 25(5):1328–1356, 2019.